Ramakrishna Mission Residential College (Autonomous)
Kolkata 700103, WB, India

Collaborative research in coordination chemistry of organic radicals

Number 7

Institute 1: Ramakrishna Mission Residential College (Autonomous)

Concerned Faculty: Dr. Prasanta Ghosh, Dept of Chemistry

&

Institute 2: **Max-Planck-Institut für Chemische Energiekonversion**

Stiftstrasse 34 - 36 / D - 45470 Mülheim an der Ruhr

Concerned Scientist: Dr Thomas Weyhermüller

Period of Investigation: 28-11-2015 to 29-05-2016

Project: o-Iminobenzoquinone and o-iminobenzosemiquinonate anion radical complexes of heavier transition Metal ions

Output: The result was published in a journal of international repute

Publication: *o*-Iminobenzoquinone and *o*-Iminobenzosemiquinonate Anion Radical Complexes of Rhodium and Ruthenium

Suvendu Maity, Suman Kundu, Sachinath Bera, Thomas Weyhermüller and Prasanta Ghosh*
Eur. J. Inorg. Chem., 2016, *22*, 3691-3697

Dr. Prasanta Ghosh

Dr Thomas Weyhermüller

ChemPubSoc Europe
DOI: 10.1002/ejic.201600526
EurJIC European Journal of Inorganic Chemistry
Full Paper

Anion Radical Complexes

o-Iminobenzoquinone and *o*-Iminobenzosemiquinonate Anion Radical Complexes of Rhodium and Ruthenium

Suvendu Maity,[a] Suman Kundu,[a] Sachinath Bera,[a] Thomas Weyhermüller,[b] and Prasanta Ghosh*[a]

Abstract: 2,4-Di-*tert*-butyl-*N*-[2-(phenylthio)]phenyl-*o*-iminobenzosemiquinonate anion radical ($L^{SPh}_{ISQ}{}^{\bullet-}$) and *o*-iminobenzoquinone (L^{SPh}_{IQ}) complexes of types *cis*-$[Rh^{III}(L^{SPh}_{ISQ}{}^{\bullet-})(PPh_3)Cl_2]$ (**1**) and *cis*-$[Ru^{II}(L^{SPh}_{IQ})(PPh_3)Cl_2]$ (**2**) are reported. The X-ray bond parameters of **2**, BS DFT calculations and variable-temperature X-band EPR spectra established the electronic states of **1**–**2**. It was verified that **1** exhibits valence tautomeric equilibria of type $[Rh^{III}(L^{SPh}_{ISQ}{}^{\bullet-})(PPh_3)Cl_2] \rightleftharpoons [Rh^{II}(L^{SPh}_{IQ})(PPh_3)Cl_2]$ (L^{SPh}_{IQ} = *o*-iminobenzoquinone state of $L^{SPh}_{ISQ}{}^{\bullet-}$) in solution. Complex **1** is unstable in moist solvent and undergoes hydrolytic C–N bond cleavage to afford $[Rh^{III}(L^{SPh}_{NH2})(PPh_3)Cl_3]$ (**3**). In solids and frozen glasses of **1** and **2**, the contributions of the "$[M^{II}(L^{SPh}_{IQ})]$" states are larger, whereas in fluid solutions the contributions of the "$[M^{III}(L^{SPh}_{ISQ}{}^{\bullet-})]$" states dominate. The contribution of the di-radical state, *cis*-$[Ru^{III}(L^{SPh}_{ISQ}{}^{\bullet-})(PPh_3)Cl_2]$, to **2** is relatively small.

Introduction

In the preceding article[1a], we report that 2,4-di-*tert*-butyl-6-{[2-(phenylthio)phenyl]amino}phenol ($L^{SPh}H_2$) is a redox-non-innocent ligand and in complexes it exists as 2,4-di-*tert*-butyl-*N*-[2-(phenylthio)]phenyl-*o*-amidophenolato ($L^{SPh}_{AP}{}^{2-}$), 2,4-di-*tert*-butyl-*N*-[2-(phenylthio)]phenyl-*o*-iminobenzosemiquinonate anion radical ($L^{SPh}_{ISQ}{}^{\bullet-}$) and the neutral 2,4-di-*tert*-butyl-*N*-[2-(phenylthio)]phenyl-*o*-iminobenzoquinone (L^{SPh}_{IQ}) states as illustrated in Scheme 1. Towards the cobalt ion, $L^{SPh}H_2$ is a bidentate NO-donor ligand that affords mixed-valence complexes of types *trans*-$[Co^{II}(L^{SPh}_{ISQ}{}^{\bullet-})(L^{SPh}_{IQ})X]$ defined by Robin–Day Class III states, *trans*-$[Co^{II}(L^{SPh}_{ISQ}{}^{0.5\bullet-})_2X]$ {X = Cl^-, SCN^-(thiocyanato-*kS*), N_3^-, NO_2^-, and I_3^-}. The existence of tautomeric equilibria of types *trans*-$[Co^{II}(L^{SPh}_{ISQ}{}^{0.5\bullet-})_2X] \rightleftharpoons$ *trans*-$[Co^{III}(L^{SPh}_{ISQ}{}^{\bullet-})_2X]$, *trans*-$[Co^{III}(L^{SPh}_{ISQ}{}^{0.5\bullet-})_2X]^+ \rightleftharpoons$ *trans*-

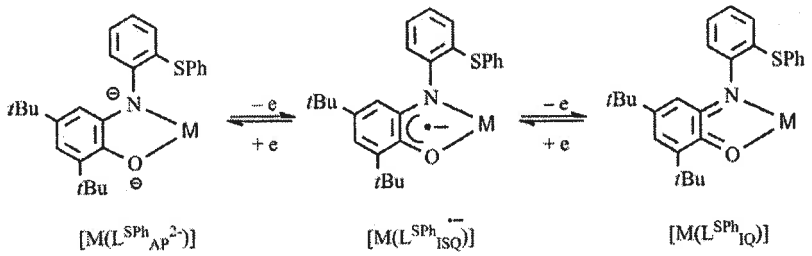

Scheme 1. Redox states of $L^{SPh}_{AP}{}^{2-}$ ligand.

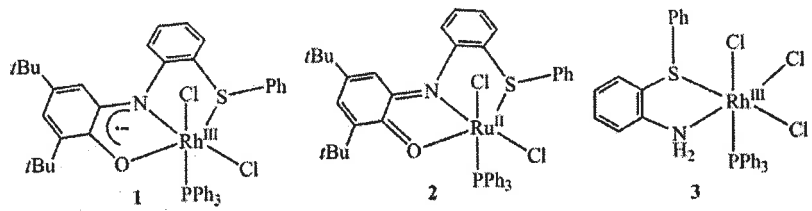

Scheme 2. Isolated complexes of rhodium and ruthenium.

[a] *Department of Chemistry, R. K. Mission Residential College, Narendrapur, Kolkata -103, India*
E-mail: ghosh@pghosh.in
www.pghosh.in
[b] *Max-Planck-Institut für Chemische Energiekonversion, Stiftstrasse 34–36, 45470 Mülheim an der Ruhr, Germany*
Supporting information for this article is available on the WWW under http://dx.doi.org/10.1002/ejic.201600526.

$[Co^{II}(L^{SPh}_{IQ})_2X]^+$, and *trans*-$[Co^{III}(L^{SPh}_{ISQ}{}^{0.5-\cdot-1.0-})_2X]^-$ ⇌ *trans*-$[Co^{II}(L^{SPh}_{ISQ}{}^{\cdot-})_2X]^-$ was verified as neutral, cation, and anion systems. In this article we disclose that $L^{SPh}H_2$ is a flexidentate redox non-innocent ligand that affords a ONS-coordinated π radical complex with rhodium(III) ion, of type *cis*-$[Rh^{III}(L^{SPh}_{ISQ}{}^{\cdot-})(PPh_3)Cl_2]$ (**1**), containing triphenyl phosphine and chloride as co-ligands, whereas it reacts with ruthenium(II) ion producing a ONS-coordinated *o*-iminobenzoquinone complex of type *cis*-$[Ru^{II}(L^{SPh}_{IQ})(PPh_3)Cl_2]$ (**2**), as illustrated in Scheme 2. The investigation revealed that **1** exhibits different electronic states in solution and as a solid because of the tautomeric equilibria of types $[Rh^{III}(L^{SPh}_{ISQ}{}^{\cdot-})(PPh_3)Cl_2]$ ⇌ $[Rh^{II}(L^{SPh}_{IQ})(PPh_3)Cl_2]$. In moist solvent, **1** hydrolyzes to $[Rh^{III}(L^{SPh}_{NH2})(PPh_3)Cl_3]$ (**3**) {L^{SPh}_{NH2} = 2-(phenylthio)aniline}. Complexes **1**–**3** were substantiated by analytical data, spectra, single-crystal X-ray structure determinations, and by density functional theory (DFT) calculations. Complex $\mathbf{2}^+$ ion was investigated by spectroelectrochemical measurements, EPR spectroscopy, and DFT calculations.

Results and Discussion

Syntheses and Characterization

Complexes **1** and **2** were prepared by using the synthetic reaction summarized in Scheme 3. Complex **1** is not stable in moist solvent and undergoes hydrolytic C–N bond cleavage affording **3**. An account in which the Rh^{III} ion promoted similar hydrolytic C–N bond cleavage was reported recently.[1b] Details of the syntheses of $L^{SPh}H_2$ and the complexes are outlined in the experimental section. The elemental analyses and the spectroscopic data are also summarized in the experimental section. In the complexes, two Cl ligands are *cis* to each other and these are abbreviated as *cis* complexes.

$$2Rh^{III}Cl_3 + 2L^{SPh}H_2 + 2PPh_3 + 1/2O_2 \longrightarrow \mathbf{1} + H_2O + 2HCl$$

$$[Ru^{II}(PPh_3)_3Cl_2] + L^{SPh}H_2 + 1/2O_2 \longrightarrow \mathbf{2} + H_2O + 2PPh_3$$

Scheme 3. Synthetic reactions of **1** and **2**.

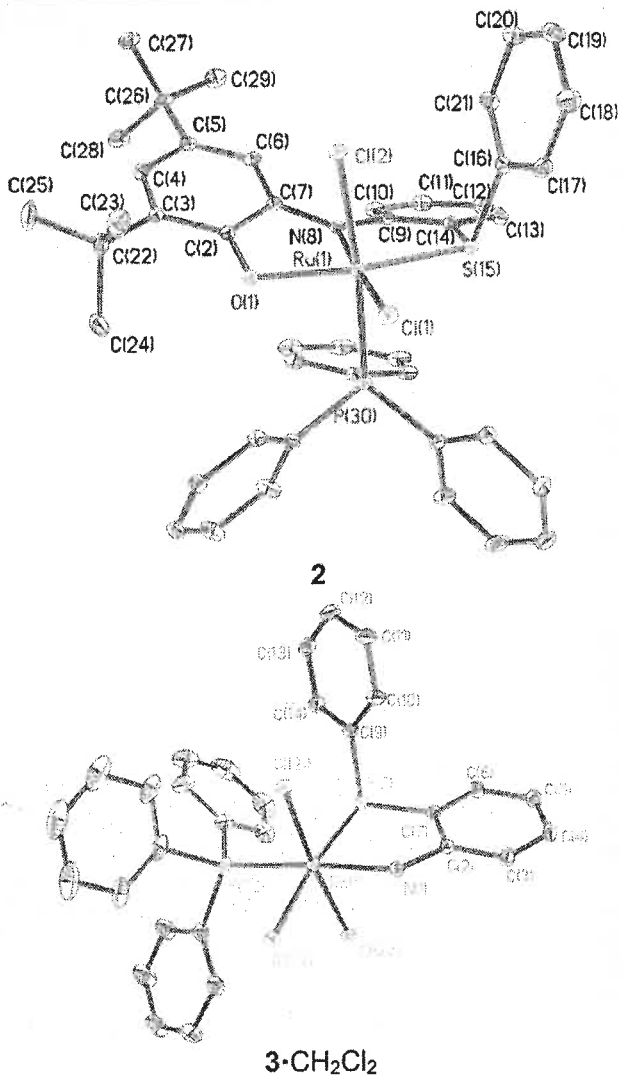

Figure 1. Molecular geometries of **2** and **3**·CH_2Cl_2 in crystals (40 % thermal ellipsoids, hydrogen atoms and solvent are omitted for clarity).

Assignment of the Electronic States

In conjunction with the X-ray bond parameters and EPR spectroscopy, DFT calculations were employed to elucidate the electronic structures of **1** and **2** and the members of their electron transfer series. The single-crystal X-ray structure determinations of **2** and **3**·CH_2Cl_2 confirmed the molecular geometries and the bond parameters of the complexes in crystals. The crystallographic data are summarized in Table S1.

The molecular geometries and the atom labeling schemes are illustrated in Figure 1. The selected bond parameters are listed in Table 1. The X-band EPR spectral parameters of **1** (solid and CH_2Cl_2 solution), are summarized in Table S2. To analyze the bond parameters and atomic spin densities, DFT calculations were performed on $[Ru(L^{SPh\text{–}tBu})(PMe_3)Cl_2]$ ($\mathbf{2}^{Me\prime}$); data for complexes $[Rh(L^{SPh\text{–}tBu})(PMe_3)Cl_2]$ ($\mathbf{1}^{Me\prime}$), $[Ru(L^{SPh\text{–}tBu})(PMe_3)Cl_2]^+$ ($\mathbf{2}^{Me\prime+}$) and the optimized coordinates are listed in Tables S4–5 ($L^{SPh\text{–}tBu}H_2$ = $L^{SPh}H_2$ ligand without *tert*-butyl substituent).

Complex **2** crystallizes in the $P\bar{1}$ space group. In **2**, the $L^{SPh}H_2$ acts as a pincer ligand and two Cl atoms are *cis* to each other. The C–O and C–N lengths are 1.294(2) and 1.356(2) Å, respectively. The C–O and C–N lengths of the *o*-amidophenolato(2–) and *o*-iminobenzosemiquinonate(1–) states of Q_{SMe} and Q_{SeMe} [Q_{SMe} = 4,6-di-*tert*-butyl-2-(2-methylthio)amidophenolate] coordinated to iridium(III)[2] and ruthenium(II)[3] ions reported by Kaim and co-workers are summarized in Table 2. The average C–O/N lengths of the Q_{SMe} and $Q_{SMe}{}^{\cdot-}$ states are 1.366 ± 0.006 and 1.341 ± 0.001 Å, respectively, whereas in **2**, these are shorter (1.325(2) Å). Thus, in crystals of **2**, a major contribution of *cis*-$[Ru^{II}(L^{SPh}_{IQ})(PPh_3)Cl_2]$ state is predicted. The dominant contribution of the Ru^{II}-quinoid state to the $[Ru(WXYZ)(bqdi)]^{n+}$ complexes was similarly elucidated by Lever and co-workers (where WXYZ are a range of spectator ligands including ammonia, phosphines, 2,2′-bipyridine, 2,2′,2″-terpyridine, carbon monoxide, water, halide, acetonitrile, triazacyclononane, nitrosyl, cyclam, etc. and bqdi = *o*-benzoquinonediimine).[4]

Table 1. Selected experimental and calculated (BS DFT) bond lengths [Å] and angles [°] of **2**, $\mathbf{2}^{Me\prime}$, and $\mathbf{2}^{Me\prime+}$.

	2 exp.	$\mathbf{2}^{Me\prime}$ calcd.	$\mathbf{2}^{Me\prime+}$ calcd.
Ru(1)–O(1)	2.062(2)	2.069	2.055
Ru(1)–N(8)	1.941(2)	1.974	2.037
Ru(1)–S(15)	2.3140(5)	2.397	2.421
Ru(1)–P(30)	2.3539(5)	2.380	2.427
Ru(1)–Cl(1)	2.3995(6)	2.454	2.344
Ru(1)–Cl(2)	2.4081(5)	2.442	2.418
O(1)–C(2)	1.294(2)	1.288	1.278
C(2)–C(7)	1.451(2)	1.457	1.474
C(7)–N(8)	1.356(2)	1.361	1.342
N(8)–C(9)	1.418(2)	1.406	1.405
C(9)–C(14)	1.406(2)	1.416	1.415
C(14)–S(15)	1.785(2)	1.801	1.796
N(8)–Ru(1)–O(1)	79.94(5)	79.73	78.36
N(8)–Ru(1)–S(15)	85.62(4)	85.07	83.49
O(1)–Ru(1)–Cl(1)	100.64(3)	99.92	106.5
S(15)–Ru(1)–Cl(1)	93.721(17)	95.57	91.59

Table 2. Experimental C–O and C–N lengths [Å] of $Q_{SMe\prime}$ $Q_{SeMe\prime}$ $Q_{SMe}^{\bullet-}$, and $Q_{SeMe}^{\bullet-}$ states reported by Kaim and co-workers.[2,3]

	C–O	C–N	avg. C–O/N
[IrCp*Q_{SMe}]	1.337(3)	1.396(4)	1.367(4)
[IrCp*$Q_{SMe}^{\bullet-}$]$^+$	1.318(6)	1.366(7)	1.342(7)
[Ru(Cym)(Q_{SMe})]	1.327(6)	1.395(6)	1.361(6)
[Ru(Cym)($Q_{SMe}^{\bullet-}$)]$^+$	1.309(3)	1.372(3)	1.340(3)
[Ru(Cym)(Q_{SeMe})]	1.332(8)	1.411(9)	1.372(8)
[Ru(Cym)($Q_{SeMe}^{\bullet-}$)]$^+$	1.312(3)	1.369(3)	1.340(3)
2	1.294(2)	1.356(2)	1.325(2)

The average Ru–Cl lengths (2.403(2) Å) of **2** are consistent with the Ru^{II}–Cl lengths. The Ru–PPh_3, Ru–S, Ru–O, and Ru–N lengths (2.354(2), 2.314(2), 2.062(2), and 1.941(2) Å, respectively) are shorter because of stronger back bonding.[5]

Analyses of the frontier orbitals of [Ru($L^{SPh\text{-}tBu}$)(PMe_3)Cl_2] ($\mathbf{2}^{Me\prime}$) revealed that the HOMO and LUMO of the singlet state scatter on both ruthenium and tridentate ONS-donor ligand. Moreover, the closed-shell singlet (CSS) solution of $\mathbf{2}^{Me\prime}$ is unstable because of open-shell singlet (OSS) perturbation. Notably, the ground-state energy of the OSS state is similar to that of the CSS state.

The calculated bond parameters of the OSS state as listed in Table 1 correlate well to these obtained from the single-crystal X-ray structure determination of **2**. The calculated average C–O/N lengths are 1.325 Å, which are similar to those found experimentally. However, the amount of alpha spin localized on the ruthenium ion is only 0.15, as shown in Figure 2. Thus, complex **2** is defined as a $L^{SPh}{}_{IQ}$ complex of ruthenium(II) of type *cis*-[Ru^{II}($L^{SPh}{}_{IQ}$)(PPh_3)Cl_2] with a minor contribution of di-radical singlet state, [Ru^{III}($L^{SPh}{}_{ISQ}^{\bullet-}$)($PPh_3$)$Cl_2$].

The EPR spectrum of a CH_2Cl_2 frozen glass sample of $\mathbf{2}^+$ was recorded at 115 K; the spectrum is shown in Figure 3 and the simulated g parameters are listed in Table S2. The g values of the $\mathbf{2}^+$ ions are consistent with those reported for ruthenium(III) complexes. This result indicates that the $\mathbf{2}^+$ ion is a $L^{SPh}{}_{IQ}$ complex of ruthenium(III) ion of type *cis*-[Ru^{III}($L^{SPh}{}_{IQ}$)(PPh_3)Cl_2]$^+$ with S = ½ spin state. The gas-phase geometry of [Ru($L^{SPh\text{-}tBu}$)(PMe_3)Cl_2]$^+$ ($\mathbf{2}^{Me\prime+}$) ion was optimized with a doublet spin state. The calculated bond parameters are summarized in Table 1 and a plot of the atomic spin densities obtained from the Mulliken spin population analyses is given in Figure 2 (b). The calculated shorter average C–O/N lengths (1.308 Å) and the exclusive localization of atomic spin at the ruthenium ion confirmed that $\mathbf{2}^+$ is a ruthenium(III) complex of $L^{SPh}{}_{IQ}$ of type *cis*-[Ru^{III}($L^{SPh}{}_{IQ}$)(PPh_3)Cl_2]$^+$.

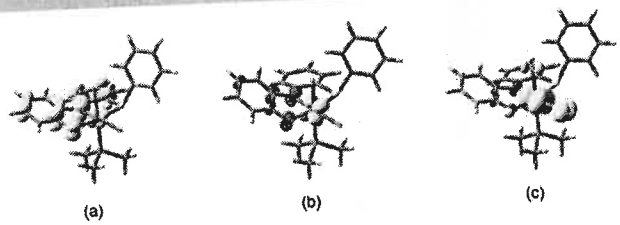

Figure 2. Atomic spin density plots of (a) $\mathbf{1}^{Me\prime}$ (Rh 0.04; O 0.18; N 0.29) and (b) $\mathbf{2}^{Me\prime}$ (Ru, 0.15; O, –0.03, N, –0.03) (c) $\mathbf{2}^{Me\prime+}$ (Ru, 0.82; Cl, 0.22) obtained from the Mulliken spin population analyses (yellow, α spin; red, β spin).

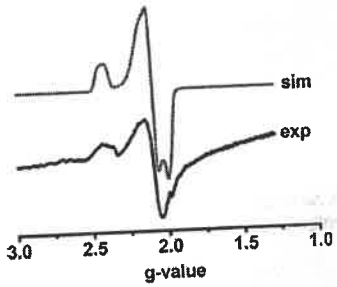

Figure 3. X-band EPR spectrum of a CH_2Cl_2 frozen-glass sample of $\mathbf{2}^+$ at 115 K.

The ground electronic state of isostructural **1** differs from that of **2**. The solid and the solution EPR spectra support the idea of a contribution of "[Rh^{II}($L^{SPh}{}_{IQ}$)]" and "[Rh^{III}($L^{SPh}{}_{ISQ}^{\bullet-}$)]" states to **1**. The X-band EPR spectrum of the solid of **1** is anisotropic, as depicted in Figure 4 (a, i). The simulated g parameters and the g-anisotropy are: g_1 = 1.962, g_2 = 2.113, g_3 = 2.325, and Δg = 0.36. The EPR spectrum was simulated by considering [Rh^{II}($L^{SPh}{}_{IQ}$)(PPh_3)Cl_2] and [Rh^{III}($L^{SPh}{}_{ISQ}^{\bullet-}$)($PPh_3$)$Cl_2$] components as shown in Scheme 4. The simulated spectrum is given in Figure 4 (a, iv). The spectrum (ii) is due to the pure component, [Rh^{II}($L^{SPh}{}_{IQ}$)(PPh_3)Cl_2], which exhibits hyperfine splitting due to one of the Cl atoms, whereas spectrum (iii) was obtained by considering an organic radical coordinated to a rhodium(III) ion as in [Rh^{III}($L^{SPh}{}_{ISQ}^{\bullet-}$)($PPh_3$)$Cl_2$]. Thus, in the solid, **1** is a hybrid state of [Rh^{II}($L^{SPh}{}_{IQ}$)(PPh_3)Cl_2] and [Rh^{III}($L^{SPh}{}_{ISQ}^{\bullet-}$)($PPh_3$)$Cl_2$] states.

As expected, **1** exhibits a valence tautomeric equilibrium in solution. The EPR spectra of **1** in CH_2Cl_2 at 115 and 296 K were recorded. The spectra are shown in Figure 4 (b) and the simulated g values are listed in Table S2. In fluid solution at 296 K, the isotropic spectrum with g = 1.995 corroborates the existence of $L^{SPh}{}_{ISQ}^{\bullet-}$ coordinated to the rhodium(III) ion, whereas in frozen glasses, the contribution of the rhodium(II) tautomer with g values, g_1 = 1.994, g_2 = 2.118, and g_3 = 2.332 dominates. In the frozen glass at 115 K, the g anisotropy is Δg = 0.34, which

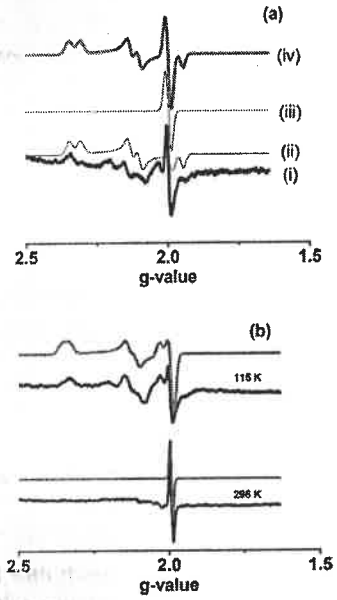

Figure 4. X-band EPR spectra of (a) solid **1** at 296 K: (i) experimental; (ii) simulated, considering the pure component $[Rh^{II}(L^{SPh}_{IQ})(PPh_3)Cl_2]$; (iii) simulated, considering the pure component of $[Rh^{III}(L^{SPh}_{ISQ}{}^{\bullet-})(PPh_3)Cl_2]$; (iv) simulated, considering 1:1 components of (ii) and (iii), and (b) CH_2Cl_2 solution of **1** (115 and 296 K).

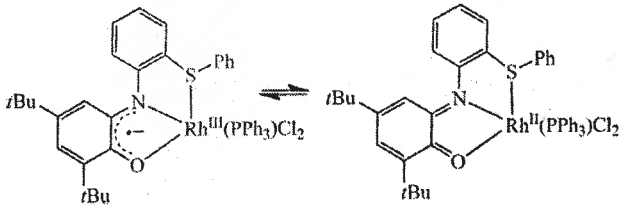

Scheme 4. Valence tautomerism (VT) of **1**.

correlates well with those of rhodium(II) complexes.[6] The feature confirms the existence of a valence tautomeric equilibrium of type $[Rh^{III}(L^{SPh}_{ISQ}{}^{\bullet-})(PPh_3)Cl_2] \rightleftharpoons [Rh^{II}(L^{SPh}_{IQ})(PPh_3)Cl_2]$, of **1** in solution, as depicted in Scheme 4.

The electronic structure of **1** was further verified by DFT calculations on $[Rh(L^{SPh\text{-}tBu})(PMe_3)Cl_2]$ ($\mathbf{1^{Me'}}$). The gas-phase geometry of $\mathbf{1^{Me'}}$ was optimized with the doublet spin state. The calculated average C–O/N lengths of $\mathbf{1^{Me'}}$ (1.332 Å), are longer than those of $\mathbf{2^{Me'}}$. The atomic spin densities, as illustrated in Figure 2 (a), are primarily localized on the ligand backbone, revealing **1** as a $L^{SPh}_{ISQ}{}^{\bullet-}$ complex of rhodium(III) of type $[Rh^{III}(L^{SPh}_{ISQ}{}^{\bullet-})(PPh_3)Cl_2]$. In comparison, the contribution of the "$[Ru^{III}(L^{SPh}_{ISQ}{}^{\bullet-})]$" state to **2** is relatively small.

Generally, *o*-iminobenzosemiquinonate anion radicals in complexes do not undergo nucleophilic substitution reactions; however, **1** undergoes a C–N bond cleavage in moist solvent affording **3**. This may be due to the existence of a tautomeric equilibrium of $[Rh^{III}(L^{SPh}_{ISQ}{}^{\bullet-})(PPh_3)Cl_2] \rightleftharpoons [Rh^{II}(L^{SPh}_{IQ})(PPh_3)Cl_2]$ states, the quinoidal state is electrophilic in nature and undergoes substitution reaction as depicted in Scheme 5. Complex **3**·CH_2Cl_2 crystallizes in the *Pbca* space group. The molecular structure in the crystal and the atom labeling scheme are depicted in Figure 1 and selected bond parameters are summarized in Table S4. With respect to three Cl atoms, the molecule has *mer* geometry. The average Rh^{III}–Cl lengths are 2.35 Å, which are shorter than the average Ru^{II}–Cl lengths in **2**. The Rh^{III}–S and Rh^{III}–P distances are similar to those of **2**. The redox activities of **1** and **2** in CH_2Cl_2 were investigated by cyclic voltammetry at 296 K. The redox potential data referenced to ferrocenium/ferrocene (Fc^+/Fc) couple are summarized in Table S5. The cyclic voltammograms are shown in Figure 5. Complex **2** exhibits one reversible anodic wave at 0.76 V because of the Ru^{III}/Ru^{II} redox couple, whereas two irreversible cathodic peaks are due to $L^{SPh}_{IQ}/L^{SPh}_{ISQ}{}^{\bullet-}$ and $L^{SPh}_{ISQ}{}^{\bullet-}/L^{SPh}_{AP}{}^{2-}$ redox couples.[7] Complex $\mathbf{2^+}$ is a ruthenium(III) complex, as predicted by the frozen glass EPR spectrum and by DFT calculations.

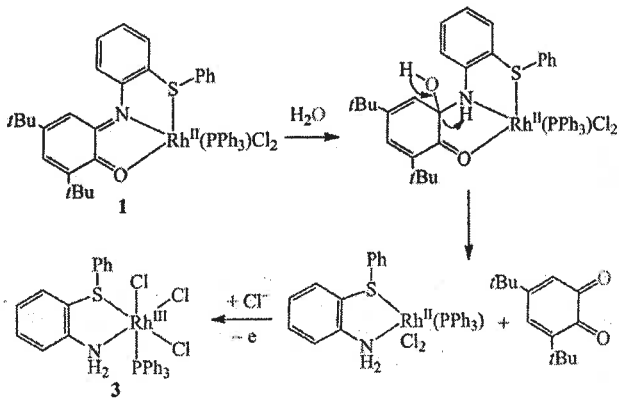

Scheme 5. Plausible paths for the C–N bond cleavage of **1**.

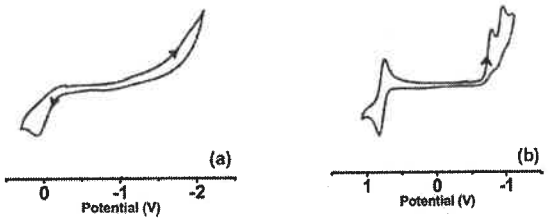

Figure 5. Cyclic voltammograms of (a) **1** and (b) **2** in CH_2Cl_2 at 296 K. Conditions: 0.2 M $[N(nBu)_4]PF_6$ supporting electrolyte; scan rate, 100 mV s^{-1}; platinum working electrode.

Electronic Spectra, Spectroelectrochemical Measurements, and Time-Dependent (TD) DFT Calculations

UV/Vis/NIR absorption spectra of **1**–**3** were recorded in CH_2Cl_2 at 296 K. The spectra are shown in Figure 6. The absorption spectroscopic data are summarized in Table S6. TD DFT calculations were employed to explore the excitation parameters of the $\mathbf{2^{Me'}}$ in CH_2Cl_2 using the CPCM model. The excitation energies with the oscillator strengths and the transition types are summarized in Table S7. The spectrum of **2** displays lower energy absorption bands at 1022 and 685 nm with a shoulder at 548 nm due to the transitions to the π_{ISQ} orbital. These transitions are absent in the free ligand. The calculated band at

1294 nm is due to the $d_{Ru} + p_{Cl} \rightarrow d_{Ru} + \pi_{ISQ}^*$ (MLCT) transition, whereas the λ_{cal} band at 680 nm is due to $d_{Ru} + p_{Cl} + \pi_{ISQ} \rightarrow d_{Ru} + \pi_{ISQ}$ (MMLLCT) transition. In solution, the absorption at 685 nm due to MMLLCT is much stronger than that at 1022 nm due to MLCT.

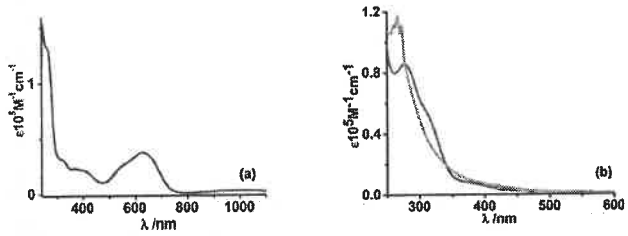

Figure 6. UV/Vis/NIR absorption spectra of (a) **2** (purple) and (b) **1** (red) and **3** (green) in CH_2Cl_2 at 296 K.

The electronic spectra of $\mathbf{2}^+$ were obtained from spectroelectrochemical measurements conducted in CH_2Cl_2 at 296 K. The change of electronic spectra with several isosbestic points during the redox reactions are shown in Figure 7.

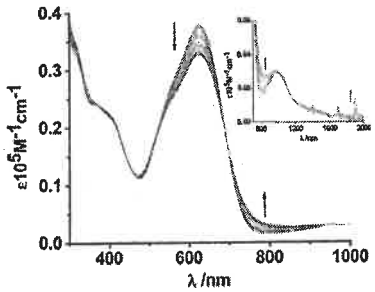

Figure 7. Spectroelectrochemical measurements showing the change of electronic spectra during the conversions of $\mathbf{2} \rightarrow \mathbf{2}^+$ in CH_2Cl_2 at 296 K.

Solid-State Electronic Spectra

The solid-state absorption spectra (Kubelka–Munk plot)[8] of **1** and **2** were recorded by using the diffuse reflection method at 296 K; the spectra are shown in Figure 8. Significant absorption peaks of the solids are summarized in Table S6. The electronic spectra of solids differ from those of CH_2Cl_2 solutions (Figure 8). The spectra of solids are broad, composed of multiple Gaussian components. They display NIR absorption bands that are absent in solutions. In solution, **1** does not exhibit any significant absorption band above 400 nm. However, in the solid state it absorbs strongly at 405–500 nm. The λ_{cal} is 471 nm, the origin of which is $d_{Rh} + p_{Cl} \rightarrow \pi_{ox}$ (MLCT) and $\pi_{ar} \rightarrow \pi_{ar}$ (ILCT) transitions. This band correlates to the existence of $[Rh^{II}(L^{SPh}{}_{IQ})(PPh_3)Cl_2]$ state in the solid, which promotes $Rh^{II} \rightarrow L^{SPh}{}_{IQ}$ and $\pi_{ar} \rightarrow L^{SPh}{}_{IQ}$ transitions. The spectrum obtained from solid **2** exhibits absorption peaks at 843, 1041, and 1430 nm. In solution, the ratio of absorbance at 1022 and 685 nm is 0.09, whereas in the solid the absorbance ratio at these two wavelengths is 1.6. Thus result infers a higher contribution of the $[Ru^{II}(L^{SPh}{}_{IQ})]$ state in the solid of **2**, which displays stronger MLCT transitions at wavelengths greater than 800 nm.

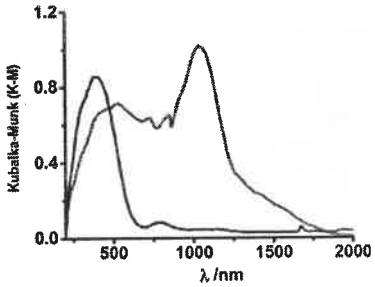

Figure 8. Solid-state UV/Vis/NIR spectra of **1** (blue) and **2** (red) at 296 K.

Conclusions

In the preceding article[1a], ligand-based mixed-valence 2,4-di-*tert*-butyl-*N*-[2-(phenylthio)]phenyl-*o*-iminobenzosemiquinonate anion radical ($L^{SPh}{}_{ISQ}^{\bullet-}$) and iminobenzoquinone ($L^{SPh}{}_{IQ}$) complexes of cobalt(II/III) ions and their valence tautomerism were reported. In this article, rhodium and ruthenium complexes of types $[Rh^{III}(L^{SPh}{}_{ISQ}^{\bullet-})(PPh_3)Cl_2]$ (**1**) and *cis*-$[Ru^{II}(L^{SPh}{}_{IQ})(PPh_3)Cl_2]$ (**2**) were established. In moist solvent, **1** undergoes hydrolytic C–N bond cleavage to afford $[Rh^{III}(L^{SPh}{}_{NH2})(PPh_3)Cl_3]$ (**3**). Complex **1** exhibits a valence tautomeric equilibrium of $[Rh^{III}(L^{SPh}{}_{ISQ}^{\bullet-})] \rightleftharpoons [Rh^{II}(L^{SPh}{}_{IQ})]$ states. In solid and frozen glass samples, **1** is a hybrid state of "$[Rh^{II}(L^{SPh}{}_{IQ})]$" and "$[Rh^{III}(L^{SPh}{}_{ISQ}^{\bullet-})]$" states, whereas in fluid solution, **1** is dominantly a $L^{SPh}{}_{ISQ}^{\bullet-}$ complex of rhodium(III). The shorter average C–O/N lengths (1.325(2) Å), the NIR MLCT absorption band in solid, and the small amount of spin density (0.15) on ruthenium ion obtained from BS DFT calculations suggest a major contribution of the nonradical $[Ru^{II}(L^{SPh}{}_{IQ})]$ state in crystals of **2**.

Experimental Section

Materials and Physical Measurements: As described in the preceding article.[1a]

2,4-Di-*tert*-butyl-6-{[2-(phenylthio)phenyl]amino}phenol ($L^{SPh}H_2$): Prepared by following a procedure described in the preceding article[1a].

***cis*-$[Rh^{III}(L^{SPh}{}_{ISQ}^{\bullet-})(PPh_3)Cl_2]$ (1):** To a solution $L^{SPh}H_2$ (200 mg, 0.5 mmol) in absolute ethanol (25 mL), $RhCl_3$ (0.5 mmol) and PPh_3 (1.2 mmol) were added successively, and the reaction mixture was heated to reflux for 40 min (351 K) under argon atmosphere. A reddish yellow solid separated out. The solution mixture was cooled to 296 K and filtered. The residue was dried in air and collected, yield 430 mg (ca. 92 % with respect to rhodium). MS (ESI, positive ion, CH_3CN): m/z = 840.27 $[1]^+$; $C_{44}H_{44}Cl_2NOPRhS$ (839.7): calcd. C 62.94, H 5.28, N 1.67; found C 62.92, H 5.27, N 1.67. IR (KBr): $\tilde{\nu}$ = 3120 (vs, *t*Bu), 3077 (vs, *t*Bu), 3042 (s, *t*Bu), 1597 (m), 1549 (s), 1481 (s), 1268 (m), 1191 (s), 695 (vs, PPh_3), 529 (vs, PPh_3) cm^{-1}.

***cis*-$[Ru^{II}(L^{SPh}{}_{IQ})(PPh_3)Cl_2]$ (2):** To a warm solution of $L^{SPh}H_2$ (40 mg, 0.1 mmol) in anhydrous toluene (30 mL) was added $[Ru(PPh_3)_3Cl_2]$ (95 mg, 0.1 mmol), and the reaction mixture was heated to reflux for 30 min. The solution became first green and then blue violet. A dark crystalline solid separated out. The reaction mixture was cooled to 296 K and filtered. The residue was dried in air and collected, yield 65 mg (ca. 77 % with respect to ruthenium). For single-

crystal X-ray structure determination, spectroscopic and electrochemical measurements, the crystals were recrystallized by diffusing *n*-hexane into a dichloromethane solution of the crude product at room temperature. MS (ESI, positive ion, CH_3OH): m/z = 801.81 [**2**–Cl]$^+$; $C_{44}H_{45}Cl_2NOPRuS$ (838.9): calcd. C 63.08, H 5.29, N 1.67; found C 63.12, H 5.27, N 1.67. ^{1}H NMR (300 MHz, $CDCl_3$): δ = 7.79 (d, 2 H), 7.66–7.75 (m, 9 H), 7.63 (s, 1 H), 7.53 (d, 4 H), 7.46 (t, 4 H), 7.25 (s, H), 7.19 (d, 2 H), 7.16 (t, 4 H), 1.55 (s, 18 H) ppm; ^{13}C NMR (75 MHz, $CDCl_3$): δ = 182.9, 167.4, 154.1, 145.7, 143.5, 133.7, 133.5, 133.2, 131.2, 131.0, 129.9, 129.5, 129.3, 129.0, 128.9, 128.6, 127.7, 127.6, 121.85, 112.3, 35.6, 34.7, 29.7, 29.1 ppm. IR (KBr): $\tilde{\nu}$ = 3055 (m, Ar–H), 2947 (s, *t*Bu), 2905 (s, *t*Bu), 2860 (m, *t*Bu), 1585 (s), 1480 (m), 1432 (s), 1298 (m), 1176 (m), 1080 (m),741 (s), 693 (s, PPh_3), 518 (s, PPh_3) cm^{-1}.

***cis*-[Rh^{III}(L^{SPh}_{NH2})(PPh_3)Cl_3] (3):** Compound **1** (84 mg, 0.1 mmol) was stirred in CH_2Cl_2 (20 mL) for 5 h at 296 K. The solution was then filtered and the filtrate was evaporated under vacuum. A yellow solid was obtained, which was thoroughly washed with boiling *n*-hexane to remove PPh_3 as one of the products. The crude product was purified on a silica gel column. Complex **3** was collected by using $CHCl_3$ as eluent. Diffusion of *n*-hexane into a dichloromethane solution of **3** generated single crystals of **3**·CH_2Cl_2 suitable for X-ray structure determination. MS (ESI, positive ion, CH_3OH): m/z = 672.32 [**3**]$^+$; $C_{30}H_{26}Cl_3NPRhS$ (672.8): calcd. C 53.55, H 3.89, N 2.08; found C 53.52, H 3.88, N 2.08. ^{1}H NMR ($CDCl_3$, 300 MHz): δ = = 8.13 (t, 2 H), 7.99 (m, 3 H), 7.79 (d, 3 H), 7.70–7.53 (m, 10 H), 7.28 (t, 3 H), 6.92 (t, 2 H), 6.49 (d, 1 H), 4.15 (s, 2 H) ppm. IR (KBr): $\tilde{\nu}$ = 3249 (m, –NH_2), 3120 (m, –NH_2), 3077 (s, Ar–H), 1597 (m), 1549 (s), 1481 (s), 1490 (m), 1436 (m), 1268 (m), 1092 (m), 744 (s), 693 (vs, PPh_3), 531 (vs, PPh_3) cm^{-1}.

Single-Crystal X-ray Structure Determination of the Complexes: Single crystals of **2** and **3**·CH_2Cl_2 were picked up with nylon loops and mounted on Bruker APEX-II CCD and Bruker AXS D8 QUEST ECO diffractometers equipped with a Mo-target rotating-anode X-ray source and a graphite monochromator (Mo-K_α, λ = 0.71073 Å). Final cell constants were obtained from least-squares fits of all measured reflections. Intensity data were corrected for absorption using intensities of redundant reflections. The structures were readily solved by direct methods and subsequent difference Fourier techniques. The crystallographic data are listed in Table S1. Siemens SHELXS-97[9] software package was used for solution, and SHELXL-97[9] was used for the refinement and XS. Ver. 2013/1,[10a] XT. Ver. 2014/4[10b] and XL. Ver. 2014/7[10c] was used for the structure solution and refinement. All non-hydrogen atoms were refined anisotropically. Hydrogen atoms were placed at the calculated positions and refined as riding atoms with isotropic displacement parameters.

CCDC 1451718 (for **1**), and 1451719 (for **2**) contain the supplementary crystallographic data for this paper. These data can be obtained free of charge from The Cambridge Crystallographic Data Centre.

DFT Calculations: All calculations reported in this article were performed with the Gaussian 03W[11] program package supported by GaussView 4.1. DFT[12] and TD DFT[13] calculations were performed at the level of Becke three parameter hybrid functional with the non-local correlation functional of Lee–Yang–Parr (B3LYP).[14] Gas-phase geometries of [Ru($L^{SPh-tBu}$)(PMe_3)Cl_2] (**2$^{Me'}$**), with singlet spin state, and [Rh($L^{SPh-tBu}$)(PMe_3)Cl_2] (**1$^{Me'}$**), [Ru($L^{SPh-tBu}$)(PMe_3)Cl_2]$^+$ (**2$^{Me'+}$**), with doublet spin state, were optimized by using Pulay's Direct Inversion[15] in the Iterative Subspace (DIIS), "tight" convergent SCF procedure[16] ignoring symmetry. As the closed shell singlet state solution of **2$^{Me'}$** was unstable, broken symmetry (BS) DFT calculations were performed to obtain stable solutions. In all calculations, a LANL2DZ basis set along with the corresponding effective core potential (ECP) was used for ruthenium, cobalt, and rhodium.[17] Valence double zeta basis set 6-31G[18] for H was used. For C, N, Cl and P, non-hydrogen atoms valence double zeta with diffuse and polarization functions, 6-31+G* as basis set[19] was employed for all calculations. The percentage contributions of metal and ligands to the frontier orbitals were calculated by using the GaussSum program package.[20] The sixty lowest singlet excitation energies on each of the optimized geometries of **2$^{Me'}$** in CH_2Cl_2 using the CPCM model[21] were calculated by using the TD DFT method.

Acknowledgments

Financial support received from the Department of Science and Technology (DST), New Delhi (SR/S1/IC/0026/2012) and Council of Scientific and Industrial Research (CSIR), New Delhi (2699/12/EMR-II). S. M., S. B., and S. K. are thankful to CSIR, India, for fellowships.

Keywords: Radical ions · Mixed-valent compounds · Tautomerism · Rhodium · C–N bond cleavage

[1] a) S. Maity, S. Kundu, S. Bera, T. Weyhermüller, P. Ghosh, *Eur. J. Inorg. Chem.* **2016**, 3680–3690. b) P. Saha, A. S. Roy, T. Weyhermüller, P. Ghosh, *Chem. Commun.* **2014**, *50*, 13073–13076.

[2] R. Hübner, S. Weber, S. Strobel, B. Sarkar, S. Záliš, W. Kaim, *Organometallics* **2011**, *30*, 1414–1418.

[3] M. Bubrin, D. Schweinfurth, F. Ehret, S. Záliš, H. Kvapilová, J. Fiedler, Q. Zeng, F. Hartl, W. Kaim, *Organometallics* **2014**, *33*, 4973–4985.

[4] A. B. P. Lever, *Coord. Chem. Rev.* **2010**, *254*, 1397–1405.

[5] M. P. Mitoraj, A. Michalak, *Inorg. Chem.* **2010**, *49*, 578–582.

[6] D. Menglet, A. M. Bond, K. Coutinho, R. S. Dickson, G. G. Lazarev, S. A. Olsen, J. R. Pilbrow, *J. Am. Chem. Soc.* **1998**, *120*, 2086–2089.

[7] H. Masui, A. B. P. Lever, P. R. Auburn, *Inorg. Chem.* **1991**, *30*, 2402–2410.

[8] P. Kubelka, F. Munk, *Z. Technol. Phys.* **1931**, *12*, 593–601.

[9] a) G. M. Sheldrick, *ShelXS97*, University of Göttingen, Germany, **1997**; b) G. M. Sheldrick, *ShelXL97*, University of Göttingen, Germany, **1997**.

[10] a) G. M. Sheldrick, XS. version 2013/1, Georg-August-Universität Göttingen, Germany, **2013**; b) G. M. Sheldrick, *Acta Crystallogr., Sect. A* **2015**, *71*, 3–8; c) G. M. Sheldrick, *Acta Crystallogr., Sect. C* **2015**, *71*, 3–8.

[11] M. J. Frisch, G. W. Trucks, H. B. Schlegel, G. E. Scuseria, M. A. Robb, J. R. Cheeseman, J. A. Montgomery Jr., T. Vreven, K. N. Kudin, J. C. Burant, J. M. Millam, S. S. Iyengar, J. Tomasi, V. Barone, B. Mennucci, M. Cossi, G. Scalmani, N. Rega, G. A. Petersson, H. Nakatsuji, M. Hada, M. Ehara, K. Toyota, R. Fukuda, J. Hasegawa, M. Ishida, T. Nakajima, Y. Honda, O. Kitao, H. Nakai, M. Klene, X. Li, J. E. Knox, H. P. Hratchian, J. B. Cross, V. Bakken, C. Adamo, J. Jaramillo, R. Gomperts, R. E. Stratmann, O. Yazyev, A. J. Austin, R. Cammi, C. Pomelli, J. W. Ochterski, P. Y. Ayala, K. Morokuma, G. A. Voth, P. Salvador, J. J. Dannenberg, V. G. Zakrzewski, S. Dapprich, A. D. Daniels, M. C. Strain, O. Farkas, D. K. Malick, A. D. Rabuck, K. Raghavachari, J. B. Foresman, J. V. Ortiz, Q. Cui, A. G. Baboul, S. Clifford, J. Cioslowski, B. B. Stefanov, G. Liu, A. Liashenko, P. Piskorz, I. Komaromi, R. L. Martin, D. J. Fox, T. Keith, M. A. Al-Laham, C. Y. Peng, A. Nanayakkara, M. Challacombe, P. M. W. Gill, B. Johnson, W. Chen, M. W. Wong, C. Gonzalez, J. A. Pople, *Gaussian 03*, revision E.01, Gaussian, Inc., Wallingford, CT, **2004**.

[12] a) R. G. Parr, W. Yang, *Density Functional Theory of Atoms and Molecules*; Oxford University Press, Oxford, U. K., **1989**; b) D. R. Salahub, M. C. Zerner, *The Challenge of d and f Electrons*, ACS Symposium Series 394, American Chemical Society, Washington, DC, **1989**; c) W. Kohn, L. J. Sham, *Phys. Rev.* **1965**, *140*, A1133–A1138; d) P. Hohenberg, W. Kohn, *Phys. Rev.* **1964**, *136*, B864–B871.

[13] a) R. E. Stratmann, G. E. Scuseria, M. Frisch, *J. Chem. Phys.* **1998**, *109*, 8218–8224; b) M. E. Casida, C. Jamoroski, K. C. Casida, D. R. Salahub, *J. Chem. Phys.* **1998**, *108*, 4439–4449; c) R. Bauernschmitt, M. Haser, O. Treutler, R. Ahlrichs, *Chem. Phys. Lett.* **1996**, *256*, 454–464.

[14] a) A. D. Becke, *J. Chem. Phys.* **1993**, *98*, 5648–5652; b) B. Miehlich, A. Savin, H. Stoll, H. Preuss, *Chem. Phys. Lett.* **1989**, *157*, 200–206; c) C. Lee, W. Yang, R. G. Parr, *Phys. Rev. B* **1988**, *37*, 785–789.
[15] P. Pulay, *J. Comput. Chem.* **1982**, *3*, 556–560.
[16] H. B. Schlegel, J. J. McDouall, in: *Computational Advances in Organic Chemistry* (Eds.: C. Ogretir, I. G. Csizmadia), Kluwer Academic, The Netherlands, **1991**.
[17] a) P. J. Hay, W. R. Wadt, *J. Chem. Phys.* **1985**, *82*, 270–283; b) W. R. Wadt, P. J. Hay, *J. Chem. Phys.* **1985**, *82*, 284–298; c) P. J. Hay, W. R. Wadt, *J. Chem. Phys.* **1985**, *82*, 299–310.
[18] a) V. A. Rassolov, M. A. Ratner, J. A. Pople, P. C. Redfern, L. A. Curtiss, *J. Comput. Chem.* **2001**, *22*, 976–984; b) M. M. Francl, W. J. Pietro, W. J. Hehre, J. S. Binkley, D. J. DeFrees, J. A. Pople, M. S. Gordon, *J. Chem. Phys.* **1982**, *77*, 3654–3665; c) P. C. Hariharan, J. A. Pople, *Mol. Phys.* **1974**, *27*, 209–214; d) P. C. Hariharan, J. A. Pople, *Theo. Chim. Acta* **1973**, *28*, 213–222; e) W. J. Hehre, R. Ditchfield, J. A. Pople, *J. Chem. Phys.* **1972**, *56*, 2257–2261.
[19] W. J. Hehre, R. Ditchfield, J. A. Pople, *J. Chem. Phys.* **1972**, *56*, 2257–2261.
[20] N. M. O'Boyle, A. L. Tenderholt, K. M. Langner, *J. Comput. Chem.* **2008**, *29*, 839–845.
[21] a) M. Cossi, N. Rega, G. Scalmani, V. Barone, *J. Comput. Chem.* **2003**, *24*, 669–681; b) V. Barone, M. Cossi, *J. Phys. Chem. A* **1998**, *102*, 1995–2001.

Received: May 5, 2016
Published Online: June 22, 2016

